

Antiferroquadrupolar and Ising-nematic orders of a frustrated bilinear-biquadratic Heisenberg model and implications for the magnetism of FeSe

Rong Yu^{1,2} and Qimiao Si³

¹*Department of Physics and Beijing Key Laboratory of Opto-electronic Functional Materials & Micro-nano Devices, Renmin University of China, Beijing 100872, China*

²*Department of Physics and Astronomy, Collaborative Innovation Center of Advanced Microstructures, Shanghai Jiaotong University, Shanghai 200240, China*

³*Department of Physics & Astronomy, Rice University, Houston, Texas 77005*

Motivated by the properties of the iron chalcogenides, we study the phase diagram of a generalized Heisenberg model with frustrated bilinear-biquadratic interactions on a square lattice. We identify zero-temperature phases with antiferroquadrupolar and Ising-nematic orders. The effects of quantum fluctuations and interlayer couplings are analyzed. We propose the Ising-nematic order as underlying the structural phase transition observed in the normal state of FeSe, and discuss the role of the Goldstone modes of the antiferroquadrupolar order for the dipolar magnetic fluctuations in this system. Our results provide a considerably broadened perspective on the overall magnetic phase diagram of the iron chalcogenides and pnictides, and are amenable to tests by new experiments.

Introduction. Because superconductivity develops near magnetic order in most of the iron pnictides and chalcogenides, it is important to understand the nature of their magnetism. The iron pnictide families typically have parent compounds which show a collinear $(\pi, 0)$ antiferromagnetic order [1]. Lowering the temperature in the parent compounds gives rise to a tetragonal-to-orthorhombic distortion, and temperature T_s for this structural transition is either equal to or larger than the Néel transition temperature T_N . A likely explanation for T_s is an Ising-nematic transition at the electronic level. It was recognized from the beginning that models with quasi-local moments and their frustrated Heisenberg $J_1 - J_2$ interactions [2] feature such an Ising-nematic transition [3–6]. Similar conclusions have subsequently been reached in models that are based on Fermi-surface instabilities [7].

The magnetic origin for the nematicity fits well with the experimental observations of the spin excitation spectrum observed in the iron pnictides. Inelastic neutron scattering experiments [8] in the parent iron pnictides have revealed a low-energy spin spectrum whose equal-intensity counters in the wavevector space form ellipses near $(\pm\pi, 0)$ and $(0, \pm\pi)$. At high energies, spin-wave-like excitations are observed all the way to the boundaries of the underlying antiferromagnetic Brillouin zone [9]. These features are well captured by Heisenberg models with the frustrated $J_1 - J_2$ interactions and bi-quadratic couplings [10, 11], although at a refined level it is also important to incorporate the damping provided by the coherent itinerant fermions near the Fermi energy [10].

Experiments in bulk FeSe do not seem to fit into this framework. FeSe is one of the canonical iron chalcogenides superconductors [12, 13]. In the single-layer limit, it currently holds particular promise towards a very high T_c superconductivity [14–16] driven by strong correlations [17]. In the bulk form, this compound displays a tetragonal-to-orthorhombic structural transition, with $T_s \approx 90$ K, but no Néel transition has been detected [18–21]. This distinction has been interpreted as pointing towards the failure of the magnetism-based origin for the structural phase transition [20, 21]. At the

same time, experiments have also revealed another aspect of the emerging puzzle. The structural transition clearly induces dipolar magnetic fluctuations [20, 21].

In this letter, we show that a generalized Heisenberg model with frustrated bilinear-biquadratic couplings on a square lattice contains a phase with both a $(\pi, 0)$ antiferroquadrupolar (AFQ) order and an Ising-nematic order. The model in this regime displays a finite-temperature transition into the Ising-nematic order and, in the presence of inter-layer couplings, also a finite-temperature transition into the AFQ order. We suggest that such physics is compatible with the aforementioned and related properties of FeSe. The Goldstone modes of the AFQ order is responsible for the onset of dipolar magnetic fluctuations near the wave-vector $(\pi, 0)$, which is experimentally testable.

Model. We consider a spin Hamiltonian with $S \geq 1$ on a two-dimensional (2D) square lattice:

$$H = \frac{1}{2} \sum_{i, \delta_n, \alpha, \beta} \{ J_n \mathbf{S}_i \cdot \mathbf{S}_j + K_n (\mathbf{S}_i \cdot \mathbf{S}_j)^2 \}, \quad (1)$$

where $j = i + \delta_n$, and δ_n connects site i and its n 's nearest neighbor sites with $n = 1, 2, 3$. Here J_n , and K_n are respectively the bilinear and biquadratic couplings between the n 's nearest neighbor spins. For the iron pnictides and chalcogenides, the local moments describe the spin degrees of freedom associated with the incoherent part of the electronic excitations and reflect the bad-metal behavior of these systems [1, 2, 4–6]. A nonzero J_3 is believed to be important for the iron chalcogenides, especially FeTe [22]. The biquadratic couplings K_n are expected to play a significant role in multi-orbital systems with moderate Hund's coupling [23]. The nearest neighbor coupling K_1 was included in previous studies [10, 11] to understand the strong anisotropic spin excitations in the Ising-nematic ordered phase, where the ground state has a $(\pi, 0)/(0, \pi)$ antiferromagnetic (AFM) order. With the goal of searching for the new physics that could describe the properties of FeSe, in this work, we take these couplings as

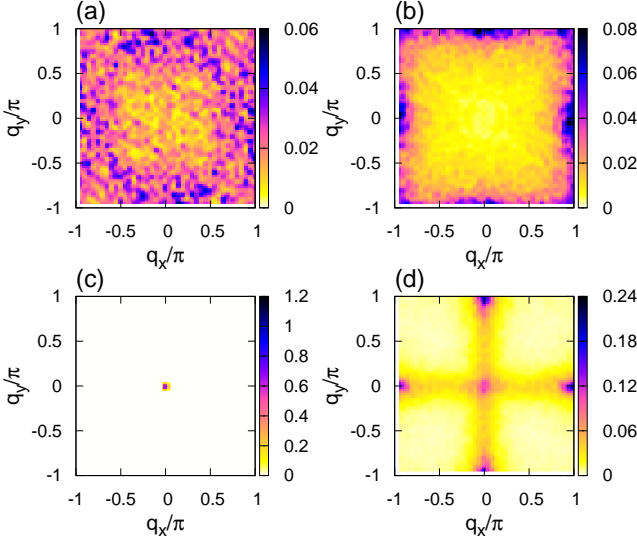


FIG. 1. Momentum distribution of the dipolar (top row) and quadrupolar (bottom row) magnetic structure factors at $K_2 = -1$ (in (a) and (c)) and $K_2 = 1.5$ (in (b) and (d)), respectively. Here, $J_1 = J_2 = 1$, $J_3 = K_3 = 0$, and $K_1 = -1$. The calculations are done on a 40×40 lattice at $T/|K_1| = 0.01$ with up to 10^5 Monte Carlo steps. In (d), besides the leading AFQ correlations at $(\pi, 0)$ and $(0, \pi)$, subleading FQ correlations are observed at finite temperatures; as the temperature is lowered, the former is enhanced whereas the latter is diminished.

variables and study the pertinent unusual phases in the phase diagram. In the following, to simplify the discussion on the relevant AFM and AFQ phases, we take $K_1 = -1$ and use $|K_1|$ as the energy unit. Note that a moderately positive K_1 in the presence of further-neighbors K_n couplings will lead to similar results, but a K_1 coupling alone in the absence of the latter will not generate the physics discussed below.

Some general considerations are in order. For $S \geq 1$,

$$(\mathbf{S}_i \cdot \mathbf{S}_j)^2 = \frac{1}{2} \mathbf{Q}_i \cdot \mathbf{Q}_j - \frac{1}{2} \mathbf{S}_i \cdot \mathbf{S}_j + \frac{1}{3} \mathbf{S}_i^2 \mathbf{S}_j^2, \quad (2)$$

where \mathbf{Q}_i is a quadrupolar operator with five components $Q_i^{x^2-3z^2} = \frac{1}{\sqrt{3}}[(S_i^x)^2 + (S_i^y)^2 - 2(S_i^z)^2]$, $Q_i^{x^2-y^2} = (S_i^x)^2 - (S_i^y)^2$, $Q_i^{xy} = S_i^x S_i^y + S_i^y S_i^x$, $Q_i^{yz} = S_i^y S_i^z + S_i^z S_i^y$, and $Q_i^{zx} = S_i^z S_i^x + S_i^x S_i^z$. Therefore, the biquadratic interaction may promote a long-range ferro/antiferro-quadrupolar (FQ/AFQ) order. With the aforementioned motivation, we are interested in a $(\pi, 0)$ AFQ order, which would break the C_4 symmetry and should yield an Ising-nematic order parameter.

Low-temperature phase diagram of the classical spin model. We first study the model in Eq. (1) for classical spins. For simplicity, we discuss the case $K_3 = 0$. We have calculated the dipolar and quadrupolar magnetic structure factors via Monte Carlo simulations using the standard Metropolis algorithm.[24] Representative results for the structure factor data are shown in Fig. 1, for $J_3 = 0$ and $J_1 = J_2$. The two cases, corresponding to different values of K_2 , show respectively dominant ferroquadrupolar (FQ) and $(\pi, 0)$ AFQ corre-

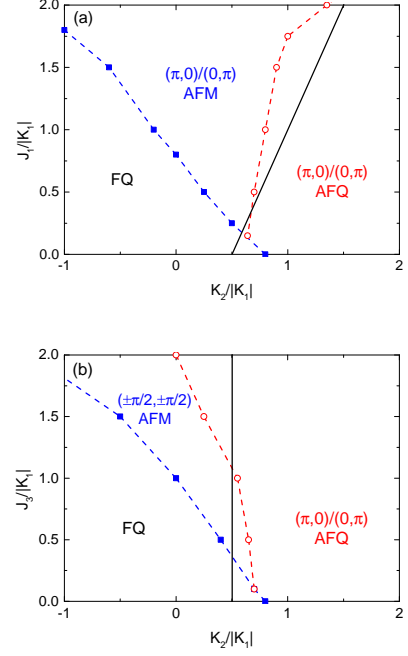


FIG. 2. Low-temperature phase diagrams of the classical bilinear-biquadratic Heisenberg model at (a): $J_1 = J_2$, $J_3 = K_3 = 0$ and (b): $J_1 = K_3 = 0$, $J_2 = J_3$. Both are shown at $T/|K_1| = 0.01$. Dashed lines show finite-temperature crossovers between different orders. The dominant order in each regime is labeled. In each case, the solid line shows the mean-field phase boundary at $T = 0$.

lations, for the finite-size systems studied and at a very low temperature $T/|K_1| = 0.01$.

Overall, as shown in Fig. 2(a), we find that there are large regimes in the phase diagram in which the FQ and $(\pi, 0)$ AFQ moments are almost ordered, while the dipolar moments coexisting with the FQ/AFQ moments are very weakly correlated. Hence in these regimes, the dominant low-temperature order is the FQ/AFQ one. In between these, there is a regime in which the dominant correlation occurs in the $(\pi, 0)$ AFM channel.

Similar results for the case of $J_1 = 0$ and $J_2 = J_3$ are shown in Fig. 2(b). A large regime with dominating FQ or $(\pi, 0)$ AFQ correlations is also found. The difference from the case of $J_3 = 0$ and $J_1 = J_2$ occurs in the regime with dominant AFM correlations, for which the wavevector is now $(\pm\pi/2, \pm\pi/2)$ as relevant to the FeTe compound.

For 2D systems, thermal fluctuations will ultimately (in the thermodynamic limit) destroy any order which breaks a continuous global symmetry at any nonzero temperature [25]. The dashed lines in Fig. 2 therefore mark crossovers between regimes with different dominant correlations. At $T = 0$, on the other hand, genuine FQ/AFQ can occur in our model on the square lattice. We have therefore also analyzed the mean-field phase diagrams at $T = 0$. The resulting phase boundary is shown in each case as a solid line in Fig. 2. The results are compatible with the crossovers identified at low but nonzero

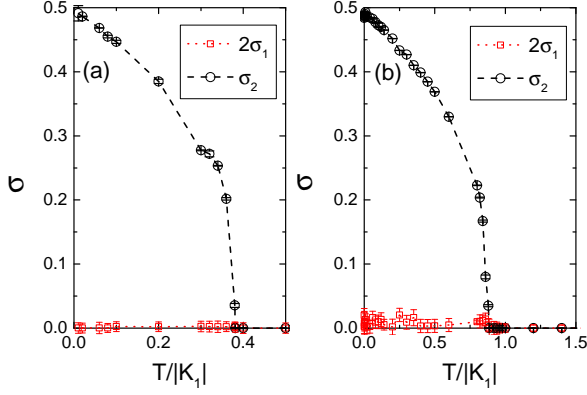


FIG. 3. (a): Temperature dependence of the Ising-nematic order parameters σ_1 and σ_2 at (a): $J_1 = J_2 = J_3 = 0$, $K_1 = -1$, and $K_2 = 1$; and (b): $J_1 = 0$, $J_2 = J_3 = 0.5$, $K_1 = -1$, and $K_2 = 2$. In both cases the dominant part of the Ising-nematic order is σ_2 , which is associated with the AFQ order.

temperatures. For the case of $J_3 = 0$ and $J_1 = J_2$, shown in Fig. 2(a), the phase on the left of the solid line has a mixture of an AFM phase ordered at $\mathbf{q} = (\pi, 0)/(0, \pi)$ and FQ phase. The phase on the right of the solid line has an AFQ phase ordered at $\mathbf{q} = (\pi, 0)/(0, \pi)$. Note that in the classical limit, the spins are treated as $O(3)$ vectors, and should always be ordered at zero temperature. We find that in the AFQ phase, the spins can be ordered at a wavevector $(q, \pi)/(\pi, q)$ for arbitrary q , with an infinite degeneracy.[26] Such a frustration would likely stabilize a purely AFQ ground state when quantum fluctuations are taken into account (see below). For the case of $J_1 = 0$ and $J_2 = J_3$, shown in Fig. 2(b), the mean-field result also yields FQ or $(\pi, 0)$ AFQ, respectively to the left or right of the solid line. However, the wave vector for the AFM orders that mix respectively with the FQ and $(\pi, 0)$ AFQ order have become $(\pm\pi/2, \pm\pi/2)$.[26]

Similar to the $(\pi, 0)$ AFM state, the $(\pi, 0)$ AFQ phase breaks the lattice C_4 rotational symmetry. An accompanying Ising-nematic transition is to be expected, and should develop at nonzero temperatures even in two dimensions. We define the general Ising-nematic operators as follows:

$$\sigma_n = (\mathbf{S}_i \cdot \mathbf{S}_{i+\hat{x}})^n - (\mathbf{S}_i \cdot \mathbf{S}_{i+\hat{y}})^n, \quad (3)$$

where $n = 1, 2$. We also introduce the quadrupolar $\mathbf{Q}_{A/B}$ to be the linear superposition of $\mathbf{Q}(\pi, 0)/(0, \pi)$, with the ratios of their coefficients to be ± 1 respectively. From Eq. (2), we see that for quantum spins, the Ising-nematic order associated with \mathbf{Q} should be seen in both σ_1 and σ_2 . For classical spins, since $\mathbf{Q}_i \cdot \mathbf{Q}_j = 2(\mathbf{S}_i \cdot \mathbf{S}_j)^2 - \frac{2}{3}\mathbf{S}_i^2\mathbf{S}_j^2$, only σ_2 will manifest $\mathbf{Q}_A \cdot \mathbf{Q}_B$. This allows us to determine the origin of the Ising-nematic order in the AFQ+AFM phase. As shown in Fig. 3(a), for the $K_1 - K_2$ model, σ_2 is ordered at $T_\sigma/|K_1| \approx 0.38$ but $\sigma_1 \approx 0$ for any $T > 0$. Likewise from Fig. 3(b), in the case $J_1 = 0$ and $J_2 = J_3$, the dominant Ising nematic order parameter is σ_2 for $T < T_\sigma \approx 0.9$, and σ_1 never becomes sub-

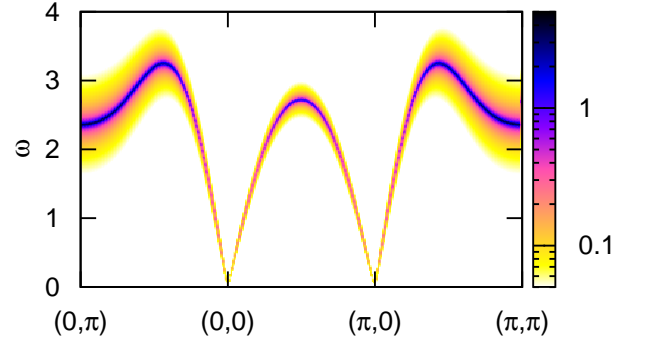


FIG. 4. Calculated spin excitation spectrum in the $(\pi, 0)$ AFQ phase of the quantum $S = 1$ model. We have taken $J_1 = J_2 = 0.25$, $J_3 = 0$, $K_2 = 0.5$, and $K_3 = -0.3$. The color codes the transverse component of the dynamical spin dipolar structure factor, $\sqrt{S_D^{xx}(\mathbf{q}, \omega)}$.

stantial down to the lowest temperature $T = 10^{-4}$ accessible to our numerical simulation. These indicate that the Ising-nematic order in the AFQ+AFM phase is associated with the anisotropic spin quadrupolar fluctuations.

The quantum spin models. The AFQ phase and the associated Ising-nematic transition are features of the generalized $J - K$ model for both classical and quantum spins. To consider the effect of quantum fluctuations, we consider the case of $S = 1$. We study its ground-state properties via a semiclassical variational approach by using an $SU(3)$ representation [27], and identify parameter regimes that stabilize the AFQ phase. We further study the spin excitations in the AFQ phase with ordering wavevector $\mathbf{q}_A = (\pi, 0)$ using a flavor-wave theory.[26] Because the AFQ order breaks the continuous spin-rotational invariance, the Goldstone modes will have non-zero dipolar matrix element [27, 28]. To explicitly demonstrate this, we calculate the dynamical spin dipolar structure factor $S_D^{xx}(\mathbf{q}, \omega)$ near \mathbf{q}_A , which is shown in Fig. 4. Therefore, the development of the AFQ order is accompanied by a sharp rise in the dynamical spin dipolar correlations centered around the wavevector $(\pi, 0)$ (and symmetry-related wave vectors).

Effects of the coupling to itinerant fermions and interaction between layers. One additional effect of the quantum fluctuations is that it can suppress the weak AFM order when the dominant order is AFQ. We discuss one source of such an effect, which is the coupling of the order parameters to the coherent itinerant fermions. The effect of coupling to the itinerant fermions can be treated as in Ref. [6] within an effective Ginzburg-Landau action, and is briefly discussed in the supplementary material [26]. When only the $(\pi, 0)$ AFM order and the Ising-nematic order are present, the coupling to the itinerant fermions will suppress the AFM and Ising-nematic order concurrently [29]. However, when the dominant order is AFQ, the coupling to the itinerant fermions can suppress the AFM order while retaining the stronger AFQ order and the associated Ising-nematic order.

When inter-layer bilinear-biquadratic couplings are taken

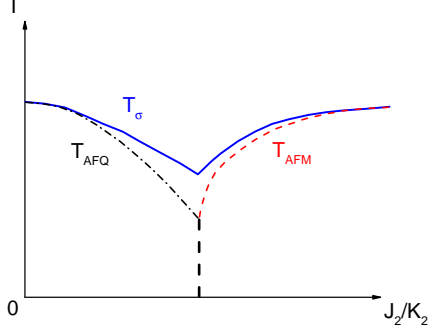


FIG. 5. (a): Schematic phase diagram in terms of T and J_2/K_2 . The dominant order may be either AFQ or AFM. The thinner dashed lines show the associated ordering temperatures T_{AFQ} and T_{AFM} . A first-order transition (thicker dashed line) takes place at an intermediate J_2/K_2 coupling when the two transitions meet. The Ising-nematic transition (solid line) takes place at T_σ . There can be either a first-order Ising-nematic and AFM(AFQ) transition at $T_\sigma = T_{AFM/AFQ}$, or two separate transitions.

into account, a phase with a pure AFQ order can be stabilized at finite temperature. We can then discuss the evolution of the Ising-nematic transition as a function of the J_2/K_2 ratio. Consider the case when a dominating J_2 stabilizes a $(\pi, 0)$ AFM order, which is accompanied by the Ising-nematic order parameter σ_1 . For sufficiently large K_2 , the AFQ becomes the dominant order, and the Ising-nematic order is predominantly given by σ_2 . The schematic evolution between the two limits is illustrated in Fig. 5. We have illustrated the case with the quantum fluctuations having suppressed the weaker order.

We stress that, such an evolution of the Ising-nematic transition already occurs in the purely 2D model. Results from explicit calculations on the evolution of the transition temperature T_σ are shown in the Supplementary Materials.[26] In the case of the Ising-nematic transition associated with a $(\pi, 0)$ AFM, the interlayer couplings gives rise to a nonzero $T_{AFM} \leq T_\sigma$ (Refs. 4–6). Similarly, when the dominant order is a $(\pi, 0)$ AFQ, such couplings lead to a nonzero $T_{AFQ} \leq T_\sigma$.

Implications for FeSe. General considerations suggest that the cases of spin 1 or spin 2 are pertinent to the iron-based materials [2]. Judging from the measured total spin spectral weight [1], the spin 1 case would be closer to the iron pnictides while the spin 2 case would be more appropriate for the iron chalcogenides.

Accordingly, it is natural to propose that the normal state of FeSe realizes the phase whose ground state has the $(\pi, 0)$ AFQ order accompanied by the Ising-nematic order. In this picture, the structural transition at $T \sim 90$ K corresponds to the concurrent Ising-nematic and AFQ transition, as illustrated in Fig. 5. This picture explains why the structural phase transition is not accompanied by any static AFM order. At

the same time, as soon as the AFQ order is developed, its Goldstone modes will contribute towards low-energy dipolar magnetic fluctuations. This is consistent with the onset of low-energy spin fluctuations observed in the NMR measurements [20, 21]. It will clearly be important to explore such spin fluctuations using inelastic neutron scattering measurements. And a quantitative comparison between the measured and calculated spin excitation spectra would allow estimates of the coupling constants J_n and K_n . The Goldstone modes may also be probed by magnetoresistance, and unusual features in this property have recently been reported [30]. Finally, the Ising-nematic order is linearly coupled not only to the structural anisotropy, but also to the orbital order. Similarly as for the iron pnictides [31], this would result in, for instance, the lifting of the d_{xz}/d_{yz} orbital degeneracy at the structural phase transition [32–34].

The phase diagrams given in Fig. 2 show that the AFQ region can be tuned to an AFM region. The nature of the AFM phase depends on the bilinear couplings. For a range of bilinear couplings, the nearby AFM phase has the ordering wavevector $(\pi/2, \pi/2)$. This provides a means to connect the magnetism of FeSe and FeTe [35, 36], which is of considerable interest to the on-going experimental efforts in studying the magnetism of the Se-doped FeTe series [37]. It also makes it natural to understand the development of magnetic order that seems to occur when FeSe is placed under a pressure on the order of 1 GPa [38–40]. Finally, we note that our results will serve as the basis to shed new light on the nematic correlations in the superconducting state [41–43].

Broader context. It is widely believed that understanding the magnetism in the iron chalcogenide FeTe, where the ordering wavevector $(\pi/2, \pi/2)$ has no connection with any Fermi-surface-nesting features [35, 36], requires a local-moment picture. The proposal advanced here not only provides an understanding of the emerging puzzle on the magnetism in FeSe, but also achieves a level of commonality in the underlying microscopic interactions across these iron chalcogenides. Furthermore, the connection between the AFQ order and the $(\pi, 0)$ AFM order suggests that the local-moment physics, augmented by a coupling to the coherent itinerant fermions near the Fermi energy, places the magnetism of a wide range of iron-based superconductors in a unified framework. Since local-moment physics in bad metals reflects a proximity to correlation-induced electron localization, this unified perspective also signifies the importance of electron correlations [2, 44–48] to the iron-based superconductors.

Conclusions. To summarize, we have studied a generalized Heisenberg model with frustrated bilinear-biquadratic interactions on a square lattice and find that the zero-temperature phase diagram stabilizes an antiferroquadrupolar order. The anisotropic spin quadrupolar fluctuations give rise to a finite-temperature Ising-nematic transition. We propose that the structural phase transition in FeSe corresponds to this Ising-nematic transition and is accompanied by an antiferroquadrupolar ordering. We suggest that inelastic neutron scattering experiments be carried out to explore the proposed

Goldstone modes associated with the antiferroquadrupolar order. Our results provide a natural understanding for an emerging puzzle on FeSe. More generally, the extended phase diagrams advanced here considerably broaden the perspective on the magnetism and electron correlations of the iron-based superconductors.

Note Added: During the final stage of preparing our manuscript, a study appeared which also emphasized the local-moment-based magnetic physics for FeSe, but invoked a different mechanism based on possible paramagnetic Ising-nematic ground state caused by J_1 - J_2 frustration [49]. A distinction of the mechanism advanced here is that the AFQ order yields Goldstone modes and therefore causes the onset of low-energy dipolar magnetic fluctuations. After the present manuscript was submitted for publication and posted on the arXiv, results from inelastic neutron scattering experiments in FeSe appeared [50, 51] which verified the $(\pi, 0)$ magnetic excitations expected from our theoretical proposal.

We would like to acknowledge an early conversation with C. Meingast, A. Böhrer and F. Hardy, which stimulated our interest in this problem, and useful discussions with E. Abrahams, B. Büchner, A. Coldea, P. Dai, D.-H. Lee and A. H. Nevidomskyy. This work was supported in part by the NSF Grant No. DMR-1309531, the Robert A. Welch Foundation Grant No. C-1411 and the Alexander von Humboldt Foundation. R.Y. was partially supported by the National Science Foundation of China Grant number 11374361, and the Fundamental Research Funds for the Central Universities and the Research Funds of Renmin University of China. Both of us acknowledge the support provided in part by the NSF Grant No. NSF PHY11-25915 at KITP, UCSB, for our participation in the Fall 2014 program on “Magnetism, Bad Metals and Superconductivity: Iron Pnictides and Beyond”. Q.S. also acknowledges the hospitality of the the Karlsruhe Institute of Technology, the Aspen Center for Physics (NSF Grant No. 1066293), and the Institute of Physics of Chinese Academy of Sciences.

-
- [1] P. Dai, J. Hu, and E. Dagotto, *Nat. Phys.* **8**, 709 (2012).
 - [2] Q. Si and E. Abrahams, *Phys. Rev. Lett.* **101**, 076401 (2008).
 - [3] P. Chandra, P. Coleman, and A. I. Larkin, *Phys. Rev. Lett.* **64**, 88 (1990).
 - [4] C. Fang *et al.*, *Phys. Rev. B* **77**, 224509 (2008).
 - [5] C. Xu, M. Muller, and S. Sachdev, *Phys. Rev. B* **78**, 020501(R) (2008).
 - [6] J. Dai *et al.*, *Proc. Natl. Acad. Sci. USA* **106**, 4118 (2009).
 - [7] R. M. Fernandes, A. V. Chubukov, and J. Schmalian, *Nat. Phys.* **10**, 97 (2014).
 - [8] S. O. Diallo *et al.*, *Phys. Rev. B* **81**, 214407 (2010).
 - [9] L. W. Harriger *et al.*, *Phys. Rev. B* **84**, 054544 (2011).
 - [10] R. Yu, Z. Wang, P. Goswami, A. H. Nevidomskyy, Q. Si and E. Abrahams, *Phys. Rev. B* **86**, 085148 (2012).
 - [11] A. L. Wysocki, K. D. Belashchenko, and V. P. Antropov, *Nat. Phys.* **7**, 485 (2011); J. P. Hu *et al.*, *Phys. Rev. B* **85**, 144403 (2012).
 - [12] F.-C. Hsu *et al.*, *Proc. Natl. Acad. Sci. USA* **105**, 14262 (2008).
 - [13] M. H. Fang *et al.*, *Phys. Rev. B* **78**, 224503 (2008).
 - [14] Q.-Y. Wang *et al.*, *Chin. Phys. Lett.* **29**, 037402 (2012).
 - [15] J.-F. Ge *et al.*, *Nat. Mater.* **10**, doi: 10.1038/nmat4153.
 - [16] J. J. Lee *et al.*, *Nature* **515**, 245 (2014).
 - [17] J. He *et al.*, *Proc. Natl. Acad. Sci. USA* **111**, 18501 (2014).
 - [18] T. M. McQueen *et al.*, *Phys. Rev. Lett.* **103**, 057002 (2009).
 - [19] S. Medvedev *et al.*, *Nat. Mater.* **8**, 630 (2009).
 - [20] A. E. Böhrer *et al.*, *Phys. Rev. Lett.* **114**, 027001 (2015).
 - [21] S.-H. Baek *et al.*, *Nat. Mater.* **14**, 210 (2015).
 - [22] F. Ma, W. Ji, J. Hu, Z.-Y. Lu, and T. Xiang, *Phys. Rev. Lett.* **102**, 177003 (2009).
 - [23] P. Fazekas, “Lecture Notes on Electron Correlation and Magnetism”, World Scientific, Singapore (1999).
 - [24] D. P. Landau and K. Binder, “A Guide to Monte Carlo Simulations in Statistical Physics”, Cambridge University Press, New York, USA (2000).
 - [25] N. D. Mermin and H. Wagner, *Phys. Rev. Lett.* **17** 1133 (1966).
 - [26] See Supplementary Materials for the exact ground state spin configurations in the AFQ phase of the classical spin model, the detailed calculation on the spin excitations of the quantum $S = 1$ model, the discussion on the effects of quantum fluctuations associated with the coupling to coherent itinerant fermions, and the evolution of the Ising-nematic transition with tuning J_2/K_2 .
 - [27] A. Läuchli, F. Mila, and K. Penc, *Phys. Rev. Lett.* **97**, 087205 (2006).
 - [28] H. Tsunetsugu and M. Arikawa, *J. Phys. Soc. Jpn.* **75**, 083701 (2006).
 - [29] J. Wu, Q. Si, and E. Abrahams, arXiv:1406.5136.
 - [30] S. Rößler *et al.*, to be published (2014).
 - [31] M. Yi *et al.*, *Proc. Natl. Acad. Sci. USA* **108**, 6878 (2011).
 - [32] K. Nakayama *et al.*, *Phys. Rev. Lett.* **113**, 237001 (2014).
 - [33] T. Shimojima *et al.*, *Phys. Rev. B* **90**, 121111(R) (2014).
 - [34] A. Coldea, talk given at the KITP program on “Magnetism, Bad Metals and Superconductivity: Iron Pnictides and Beyond”, <http://online.kitp.ucsb.edu/online/ironic14/coldea/>.
 - [35] W. Bao *et al.*, *Phys. Rev. Lett.* **102**, 247001 (2009).
 - [36] S. Li *et al.*, *Phys. Rev. B* **79**, 054503 (2009).
 - [37] J. Tranquada, talk given at the KITP conference on “Strong Correlations and Unconventional Superconductivity”, <http://online.kitp.ucsb.edu/online/ironic-c14/tranquada/>.
 - [38] M. Bendele *et al.*, *Phys. Rev. Lett.* **104**, 087003 (2010).
 - [39] M. Bendele *et al.*, *Phys. Rev. B* **85**, 064517 (2012).
 - [40] T. Imai *et al.*, *Phys. Rev. Lett.* **102**, 177005 (2009).
 - [41] C.-L. Song *et al.*, *Science* **332**, 1410 (2011).
 - [42] H.-H. Hung, C.-L. Song, X. Chen, X. Ma, Q.-K. Xue and C. Wu, *Phys. Rev. B* **85**, 104510 (2012).
 - [43] D. Chowdhury, E. Berg and S. Sachdev, *Phys. Rev. B* **84**, 205113 (2011).
 - [44] Z. P. Yin, K. Haule, and G. Kotliar, *Nature Mater.* **10**, 932 (2011).
 - [45] K. Seo, B. A. Bernevig and J. Hu, *Phys. Rev. Lett.* **101**, 206404 (2008).
 - [46] A. Moreo, M. Daghofer, J. A. Riera, and E. Dagotto, *Phys. Rev. B* **79**, 134502 (2009).
 - [47] W. Lv, F. Krüger, and P. Phillips, *Phys. Rev. B* **82**, 045125 (2010).
 - [48] R. Yu *et al.*, *Nat. Commun.* **4**, 2783 (2013).
 - [49] F. Wang, S. Kivelson, and D.-H. Lee, arXiv:1501.00844.
 - [50] M. C. Rahn *et al.*, arXiv:1502.03838.
 - [51] Q. Wang *et al.*, arXiv:1502.07544.

SUPPLEMENTARY MATERIAL

The ground-state spin configurations in the classical spin model

Exactly at $T = 0$, the classical $O(3)$ spins are always ordered. Therefore, the AFQ order is accompanied by magnetic dipolar orders. Because the $(\pi, 0)$ AFQ order doubles the unit cell, the structure factor $\mathcal{S}_D(\mathbf{q})$ of the compatible magnetic dipolar order must show a two- q structure as the consequence of Brillion zone folding, *i.e.*, $\mathcal{S}_D(\mathbf{q}) = \mathcal{S}_D(\mathbf{q} + \mathbf{q}_A)$ where $\mathbf{q}_A = (\pi, 0)$. The ordering wavevector \mathbf{q} depends on model parameters.

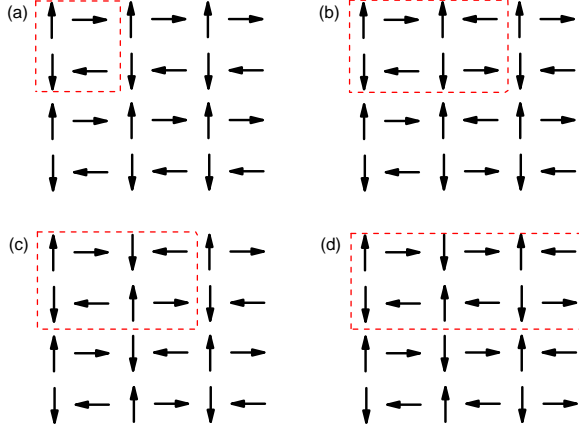


FIG. S1. Four among the infinitely degenerate ground-state spin patterns in the case of $J_3 = 0$ and $J_1 = J_2$. In each case, the dashed box shows the magnetic unit cell. The corresponding ordering wavevectors are as follows: $\mathbf{q} = (0, \pi)$ and (π, π) in (a); $\mathbf{q} = (\pm\pi/2, \pi)$ in (b) and (c); $\mathbf{q} = (2\pi/3, \pi)$ and $(-\pi/3, \pi)$ in (d).

We find that in the $(\pi, 0)/(0, \pi)$ AFQ ground state the spins are ordered at a wavevector $(q, \pi)/(\pi, q)$ with infinite degeneracies for $J_3 = 0$. Assuming a $(\pi, 0)$ AFQ order, the spin variable at site i is $\mathbf{S}_i = \xi(i_x)[\hat{e}_x\gamma(i_x) + \hat{e}_y(1 - \gamma(i_x))]\gamma(i_y)$, where i_x and i_y are coordinates of site i , $\gamma(i_{x(y)}) = (1 + (-1)^{i_{x(y)}})/2$, and $\xi(i_x) = \pm 1$ is a random variable defined on each column of the lattice. The randomness in the real-space spin configuration leads to infinite number of degenerate ground-state spin patterns. Transforming to the momentum space, they correspond to ordering wavevector at (q, π) (and $(q + \pi, \pi)$) with q an arbitrary number. Some of the degenerate spin patterns are shown in Fig. S1.

As for the case of $J_1 = 0$ and $J_2 = J_3$, in the AFQ phase, we still find 16-fold degenerate ground-state spin patterns at ordering wavevectors $(\pm\pi/2, \pm\pi/2)$. Some of the spin patterns are shown in Fig. S2. In both cases, the large number of degenerate classical spin ground states helps to stabilize an AFQ order without a magnetic dipolar one when the quantum fluctuations are taken into account.

Another interesting observation is that at $T = 0$, the dominant $(\pi, 0)$ AFQ order of $Q^{x^2-y^2}$ coexists with a subleading FQ order of $Q^{r^2-3z^2}$. This can be checked using the

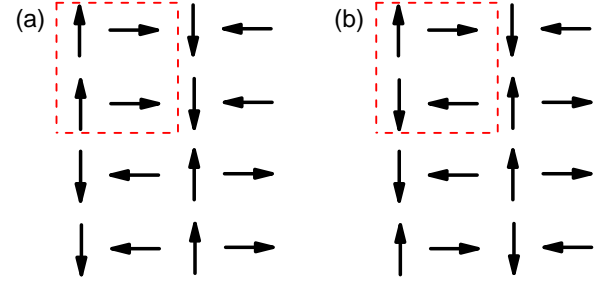


FIG. S2. Two out of the 16 degenerate ground-state spin patterns in the case of $J_1 = 0$ and $J_2 = J_3$. In each case, the spin pattern can be obtained by repeatedly aligning the spins in the dashed box in a staggered way. In both cases, the ordering wavevectors are $\mathbf{q} = (\pm\pi/2, \pm\pi/2)$.

ground-state spin configurations in Figs. S1 and S2, which gives $Q_i^{r^2-3z^2} = 1/\sqrt{3}$ at each site and $Q^{x^2-y^2} = \pm 1$.

Spin excitations and Goldstone modes in the quantum $S = 1$ model

For the case of quantum spin $S = 1$, the model defined in Eq. (1) of the main text can be studied by an $SU(3)$ Schwinger boson approach.[1] At each site, let $|-1\rangle$, $|0\rangle$, and $|1\rangle$ be the three eigenstates of the spin operator S^z . We can define a time-reversal invariant basis of the $SU(3)$ representation:

$$\begin{aligned} |x\rangle &= \frac{i}{\sqrt{2}} (|1\rangle - |-1\rangle), \\ |y\rangle &= \frac{1}{\sqrt{2}} (|1\rangle + |-1\rangle), \\ |z\rangle &= -i|0\rangle. \end{aligned} \quad (S1)$$

Within this representation, we can then define three Schwinger bosons associated with the above three states, $b_\alpha^\dagger|\emptyset\rangle = |\alpha\rangle$, where $\alpha = x, y, z$, and $|\emptyset\rangle$ is the null state of the Schwinger bosons. The three bosons satisfy a local constraint at each site:

$$\sum_{\alpha} b_{i\alpha}^\dagger b_{i\alpha} = 1. \quad (S2)$$

The spin dipolar and quadrupolar operators can be written in terms of the Schwinger boson bilinears as

$$S_i^\alpha = -i\epsilon_{\alpha\beta\gamma}(b_{i\beta}^\dagger b_{i\gamma} - b_{i\gamma}^\dagger b_{i\beta}), \quad (S3)$$

$$\begin{aligned} Q_i^{\alpha\beta} &= -(b_{i\alpha}^\dagger b_{i\beta} + b_{i\beta}^\dagger b_{i\alpha}), \\ Q_i^{x^2-y^2} &= -(b_{ix}^\dagger b_{ix} - b_{iy}^\dagger b_{iy}), \\ Q_i^{r^2-3z^2} &= \frac{1}{\sqrt{3}}(2b_{iz}^\dagger b_{iz} - b_{ix}^\dagger b_{ix} - b_{iy}^\dagger b_{iy}), \end{aligned} \quad (S4)$$

where α, β , and γ run over x, y , and z , and $\epsilon_{\alpha\beta\gamma}$ is the Levi-Civita symbol. The Hamiltonian is then rewritten as

$$H = \frac{1}{2} \sum_{i, \delta_n, \alpha, \beta} \left\{ J_n b_{i\alpha}^\dagger b_{j\alpha} b_{j\beta}^\dagger b_{i\beta} + (K_n - J_n) b_{i\alpha}^\dagger b_{j\alpha}^\dagger b_{j\beta} b_{i\beta} \right\}, \quad (\text{S5})$$

where $j = i + \delta_n$, and δ_n (with $n = 1, 2, 3$) connects site i and its n 's nearest neighbor sites.

We assume the following ground state at the mean level: $|\psi\rangle = \Pi_i |\psi_i\rangle = \Pi_i \sum_{\alpha} f_{i\alpha} b_{i\alpha}^\dagger |\emptyset\rangle$, where the coefficients satisfy $\sum_{\alpha} |f_{i\alpha}|^2 = 1$. The $(\pi, 0)$ AFQ order can be obtained by requiring condensation of b_x and b_y bosons at sites in odd and even columns, respectively. Correspondingly, the mean-field ground-state wave function at site i is $|\psi_i\rangle = |x\rangle_i$ if the x coordinate of site i (i_x) is odd, and $|\psi_i\rangle = |y\rangle_i$ if i_x is even. One could check that this wave function is indeed associated to an AFQ order at wavevector $\mathbf{q}_A = (\pi, 0)$ since $\langle \psi_i | Q^{x^2-y^2} | \psi_i \rangle = e^{\mathbf{q}_A \cdot \mathbf{r}_i} = \pm 1$.

We study the spin excitations in the AFQ phase by using a flavor-wave theory. We first perform a local rotation in the spin space,

$$\begin{pmatrix} d_{ix} \\ d_{iy} \\ d_{iz} \end{pmatrix} = \begin{pmatrix} \cos \theta_i & \sin \theta_i & 0 \\ -\sin \theta_i & \cos \theta_i & 0 \\ 0 & 0 & 1 \end{pmatrix} \begin{pmatrix} b_{ix} \\ b_{iy} \\ b_{iz} \end{pmatrix}, \quad (\text{S6})$$

such that in the rotated basis, only one flavor of bosons, d_{ix} , condenses. In the $(\pi, 0)$ AFQ phase, this corresponds to taking $\theta_i = 0$ if i_x is odd and $\theta_i = \pi/2$ if i_x is even. Using the constraint in this rotated basis, $\sum_{\alpha} d_{i\alpha}^\dagger d_{i\alpha} = 1$, we obtain

$$\begin{aligned} d_{ix} &\rightarrow \sqrt{1 - d_{iy}^\dagger d_{iy} - d_{iz}^\dagger d_{iz}} \\ &\approx 1 - \frac{1}{2} (d_{iy}^\dagger d_{iy} + d_{iz}^\dagger d_{iz}). \end{aligned} \quad (\text{S7})$$

Using Eq. (S7), we can rewrite the Hamiltonian in Eq. (S5) in terms of the magnon operators b_{iy} and b_{iz} . Expanding the Hamiltonian up to the quadratic terms of the magnon operators, then Fourier transforming it to the momentum space, we arrive at, up to a constant energy,

$$\begin{aligned} H \approx \sum_{k, \alpha=y, z} A_{k\alpha} (d_{k\alpha}^\dagger b_{k\alpha} + d_{-k\alpha} b_{-k\alpha}^\dagger) \\ + B_{k\alpha} (d_{k\alpha}^\dagger d_{-k\alpha}^\dagger + d_{k\alpha} d_{-k\alpha}). \end{aligned} \quad (\text{S8})$$

Here k runs over the unfolded Brillouin zone (BZ), and

$$\begin{aligned} A_{ky} &= J_1 (\cos k_x + \cos k_y) - K_1 \cos k_x \\ &\quad - 2(K_2 - J_2) \cos k_x \cos k_y + J_3 (\cos 2k_x + \cos 2k_y) \\ &\quad + 2K_2 - 2K_3, \end{aligned} \quad (\text{S9})$$

$$\begin{aligned} B_{ky} &= K_1 \cos k_y - J_1 (\cos k_x + \cos k_y) - 2J_2 \cos k_x \cos k_y \\ &\quad + (K_3 - J_3) (\cos 2k_x + \cos 2k_y), \end{aligned} \quad (\text{S10})$$

$$A_{kz} = J_1 \cos k_y + J_3 (\cos 2k_x + \cos 2k_y) - K_1 - 2K_3, \quad (\text{S11})$$

$$B_{kz} = (K_1 - J_1) \cos k_y + (K_3 - J_3) (\cos 2k_x + \cos 2k_y). \quad (\text{S12})$$

The Hamiltonian in Eq. (S8) can be diagonalized via a Bogoliubov transformation

$$d_{ky(z)} = u_{ky(z)} \gamma_{ky(z)} - v_{ky(z)} \gamma_{ky(z)}^\dagger, \quad (\text{S13})$$

and

$$H \approx \sum_{k, \alpha=y, z} \epsilon_{k\alpha} (\gamma_{k\alpha}^\dagger \gamma_{k\alpha} + \gamma_{-k\alpha} \gamma_{-k\alpha}^\dagger), \quad (\text{S14})$$

where the magnon dispersion

$$\epsilon_{k\alpha} = \sqrt{A_{k\alpha}^2 - B_{k\alpha}^2}, \quad (\text{S15})$$

and

$$\begin{aligned} u_{k\alpha} &= \frac{1}{2} \left(\frac{A_{k\alpha}}{\sqrt{A_{k\alpha}^2 - B_{k\alpha}^2}} + 1 \right), \\ v_{k\alpha} &= \frac{1}{2} \left(\frac{A_{k\alpha}}{\sqrt{A_{k\alpha}^2 - B_{k\alpha}^2}} - 1 \right). \end{aligned} \quad (\text{S16})$$

The parameter regime where the $(\pi, 0)$ AFQ phase is stable is obtained by requiring $A_{k\alpha} \geq 0$ and $A_{k\alpha}^2 - B_{k\alpha}^2 \geq 0$ at every k in the entire BZ and for both $\alpha = y, z$, and can be determined numerically.

The dynamical spin dipolar and quadrupolar structure factors $S_Q^{\mu\mu}(\mathbf{q}, \omega)$ and $S_D^{\alpha\alpha}(\mathbf{q}, \omega)$ can be calculated within the diagonalized representation. In general,

$$S_Q^{\mu\mu}(\mathbf{q}, \omega) = \sum_m |\langle g | Q_{\mathbf{q}}^\mu | m \rangle|^2 \delta(\omega - (E_m - E_g)), \quad (\text{S17})$$

$$S_D^{\alpha\alpha}(\mathbf{q}, \omega) = \sum_m |\langle g | S_{\mathbf{q}}^\alpha | m \rangle|^2 \delta(\omega - (E_m - E_g)). \quad (\text{S18})$$

Here, $|g\rangle$ and $|m\rangle$ refer to the ground state (with eigenenergy E_g) and the m 's excited state (with eigenenergy E_m) in the flavor-wave theory.

$$Q_{\mathbf{q}}^\mu = \frac{1}{\sqrt{N}} \sum_i e^{i\mathbf{q} \cdot \mathbf{r}_i} Q_i^\mu, \quad (\text{S19})$$

$$S_{\mathbf{q}}^\alpha = \frac{1}{\sqrt{N}} \sum_i e^{i\mathbf{q} \cdot \mathbf{r}_i} S_i^\alpha, \quad (\text{S20})$$

where N is the number of spins of the system, and Q_i^μ and S_i^α are expressed in terms of Schwinger bosons using Eqs. (S3) and (S4). For example, for $\mu = x^2 - y^2$,

$$Q_{\mathbf{q}}^{x^2-y^2} = \sqrt{N}\delta_{\mathbf{q},\mathbf{q}_A} - \frac{2}{\sqrt{N}} \sum_k d_{ky}^\dagger d_{k+\mathbf{q}+\mathbf{q}_A,y} - \frac{1}{\sqrt{N}} \sum_k d_{kz}^\dagger d_{k+\mathbf{q}+\mathbf{q}_A,z}. \quad (\text{S21})$$

This leads to $S_Q^{\mu\mu}(\mathbf{q}, \omega) = N\delta_{\mathbf{q},\mathbf{q}_A}\delta(\omega)$ up to the one-magnon contribution, which confirms the AFQ order at $\mathbf{q}_A = (\pi, 0)$.

The one-magnon contribution to the spin dipolar correlation function is also non-zero. We find that the transverse dynamical structure factor

$$S_D^{xx}(\mathbf{q}, \omega) = S_D^{yy}(\mathbf{q}, \omega) = \frac{1}{2} \sqrt{\frac{A_{\mathbf{q}z} + B_{\mathbf{q}z}}{A_{\mathbf{q}z} - B_{\mathbf{q}z}}} \delta(\omega - \epsilon_{\mathbf{q}z}) \quad (\text{S22})$$

From Eqs. (S11), (S12), and (S15), we find a Goldstone mode near $\mathbf{q}_A = (\pi, 0)$. For $\mathbf{q} = \mathbf{q}_A + (dq_x, dq_y)$,

$$\epsilon_{\mathbf{q}z} \approx \sqrt{v_x^2 dq_x^2 + v_y^2 dq_y^2}, \quad (\text{S23})$$

with anisotropic velocities

$$v_x = 2\sqrt{K_3\eta}, \quad v_y = \sqrt{(K_1 + 4K_3)\eta}, \quad (\text{S24})$$

where $\eta = K_1 + 2K_3 - J_1 - 2J_3$. The Goldstone mode near \mathbf{q}_A is also seen in the dynamical spin dipolar structure factor:

$$S_D^{xx}(\mathbf{q} \rightarrow \mathbf{q}_A, \omega) \approx \frac{\omega}{2\eta} \delta(\omega - \epsilon_{\mathbf{q}z}). \quad (\text{S25})$$

Note that the static dipolar structure factor $S_D^{xx}(\mathbf{q}_A) = 0$, because of the absence of long-range magnetic dipolar order in the AFQ phase. But the Goldstone modes associated with the broken spin rotational symmetry can be observed from the dynamical spin dipolar structure factor. A representative plot of $S_D^{xx}(\mathbf{q}, \omega)$ showing the Goldstone modes is displayed in Fig. 4 of the main text.

Quantum fluctuations and coupling to itinerant fermions.

The field theory that describes the two coupled order parameters \mathbf{Q}_A and \mathbf{Q}_B will be similar to that of the $(\pi, 0)$ AFM order of the $J_1 - J_2$ Heisenberg model. The effect of coupling to the itinerant fermions can be treated as in Ref. [2] within an effective Ginzburg-Landau action:

$$\begin{aligned} \mathcal{S}(\mathbf{Q}_A, \mathbf{Q}_B) &= \int d\{\mathbf{q}\} \int d\{\omega\} [\mathcal{S}_2 + \mathcal{S}_4 + \dots], \\ \mathcal{S}_2(\mathbf{q}, \omega) &= r(\omega, \mathbf{q})[|\mathbf{Q}_A(\mathbf{q}, \omega)|^2 + |\mathbf{Q}_B(\mathbf{q}, \omega)|^2] \\ &\quad + v(q_x^2 - q_y^2)[\mathbf{Q}_A(\mathbf{q}, \omega) \cdot \mathbf{Q}_B(-\mathbf{q}, -\omega)], \\ \mathcal{S}_4(\{\mathbf{q}\}, \{\omega\}) &= u(|\mathbf{Q}_A|^4 + |\mathbf{Q}_B|^4) + u'|\mathbf{Q}_A|^2 |\mathbf{Q}_B|^2 \\ &\quad + \tilde{u}|\mathbf{Q}_A \cdot \mathbf{Q}_B|^2. \end{aligned} \quad (\text{S26})$$

where $r(\omega, \mathbf{q}) = r_0 + wA + \omega^2 + \gamma|\omega| + cq^2$, $r_0 < 0$ and $A > 0$ are constants, w is the coherent quasiparticle spectral weight of itinerant electrons, and γ is a Landau-damping coefficient. Note that $\tilde{u} < 0$, and $\{\mathbf{q}\}, \{\omega\}$ mark the set of four momenta and four frequencies that enter \mathcal{S}_4 ; the momentum and frequency integrals are understood to each contain a delta function that fixes the sum of the momenta and the sum of the frequencies at zero. A similar form also exists for the AFM orders, \mathbf{M}_A and \mathbf{M}_B [2]. The shift of r by w and the damping may lead to the loss of magnetic order in the system [2], and stabilize a pure AFQ order. In the absence of the AFQ order, the Ising-nematic order will be concurrently suppressed [3]. However, when the dominant order is AFQ, one can readily reach the regime where the quantum fluctuations eliminate the weaker AFM order while retaining the stronger AFQ order and the associated Ising-nematic order.

The evolution of the Ising-nematic order parameter and transition temperature as a function of J_2/K_2

Here we study how the dominant Ising-nematic order parameter and the associated transition temperature, T_σ , change with varying the J_2/K_2 ratio in the 2D classical bilinear-biquadratic Heisenberg model. The calculations are done via classical Monte Carlo simulations using Metropolis sampling with up to 80×80 lattices and 10^5 Monte Carlo steps.

We tune the J_2/K_2 ratio by going along the blue dashed trajectory in the phase diagram shown in Fig. S3(a). As discussed in the main text, with increasing K_2 , the ground state of the system changes from the $(\pi, 0)/(0, \pi)$ AFM to the $(\pi, 0)/(0, \pi)$ AFQ state. We have tracked the evolution of the Ising-nematic order parameters σ_1 and σ_2 , and find that the change of the ground state is reflected in the variation of the Ising-nematic order parameters: the dominant Ising-nematic order parameter changes from σ_1 in the AFM phase to σ_2 in the AFQ phase, as clearly shown in Fig. S3(b) and (c). We have also determined the transition temperature T_σ from our numerical results. T_σ first decreases then increases with increasing K_2 along the trajectory, showing a remarkable minimum near the phase boundary between the AFM and AFQ phases (Fig. S3(d)). This minimum indicates enhanced fluctuations around the Ising-nematic order due to the competition between the AFM and AFQ orders. Our results on the evolution of the dominant Ising-nematic order parameter and T_σ with J_2/K_2 are fully consistent with the general picture proposed in Fig. 5 of the main text. When an interlayer coupling is turned on, we expect similar results for the Ising-nematic order, because the change of the dominant Ising-nematic order parameter and the evolution of T_σ reflect the competition between the underlying AFM and AFQ ground states. In this case, in the dominating AFM regime, it is well known that a nonzero transition temperature develops for the AFM order. Similar reasoning applies to the dominating AFQ regime.

-
- [1] A. Läuchli, F. Mila, and K. Penc, Phys. Rev. Lett. **97**, 087205 (2006).
- [2] J. Dai *et al.*, Proc. Natl. Acad. Sci. USA **106**, 4118 (2009).
- [3] J. Wu, Q. Si, and E. Abrahams, arXiv:1406.5136.

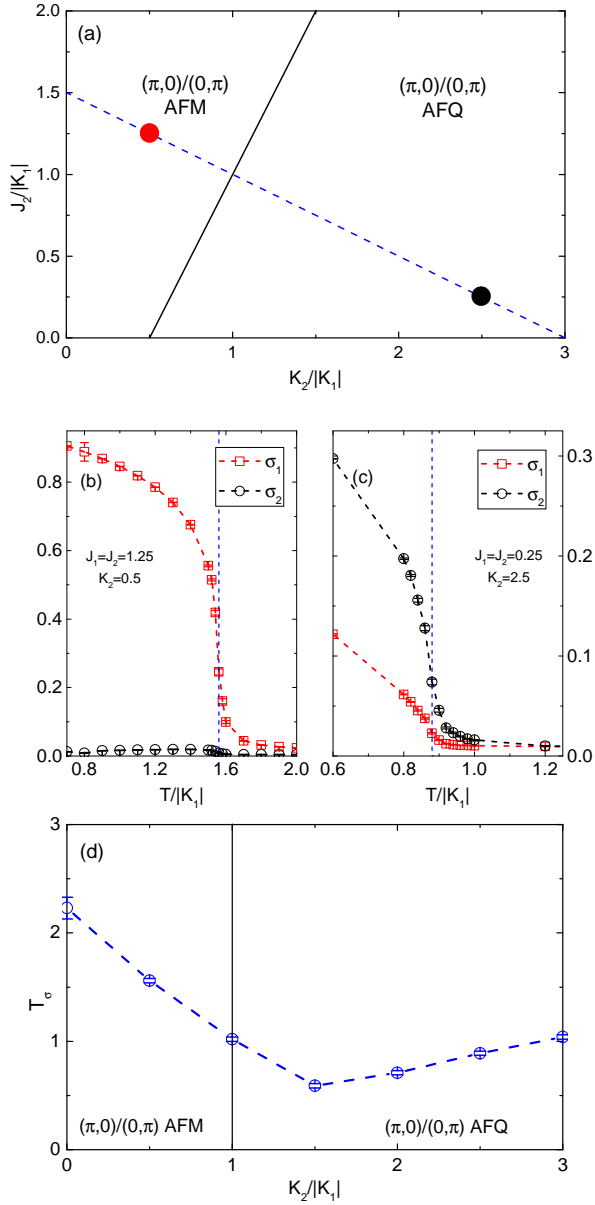


FIG. S3. (a): Mean-field ground-state phase diagram of the classical bilinear-biquadratic Heisenberg model at $J_3 = K_3 = 0$ and $J_1 = J_2$. The blue dashed line shows the trajectory by tuning J_2/K_2 , and the red and black dots show two representative points along this trajectory. (b) and (c): Temperature dependence of the Ising-nematic order parameters σ_1 and σ_2 at the two representative points of the phase diagram in panel (a). There is a change of the dominant Ising-nematic order parameter from σ_1 to σ_2 when the ground state varies from the AFM to the AFQ phase. The blue dashed line marks the transition temperature, T_σ , of the Ising-nematic transition. Data shown are based on Monte Carlo simulations on a 40×40 lattice. (d): Evolution of T_σ with varying J_2/K_2 along the trajectory shown in panel (a). A minimum of T_σ is located near the phase boundary (black solid line) between the AFM and the AFQ phase, which is consistent with the proposal made in the main text, as illustrated in Fig. 5 of the main text.